



# Numerical study on the effect of grain size on rock dynamic tensile properties using PFC-GBM

Li Wangyang<sup>1,2</sup> · Shi Chong<sup>1,2</sup> · Zhang Cong<sup>1,2</sup>

Received: 11 April 2023 / Revised: 13 June 2023 / Accepted: 25 June 2023 / Published online: 11 July 2023  
© The Author(s) under exclusive licence to OWZ 2023

## Abstract

To understand the effect of grain size on the rock dynamic mechanical behaviors, dynamic semi-circular bending (SCB) experiments were carried out by means of a grain-based model based on particle flow code (PFC-GBM) with a split Hopkinson pressure bar (SHPB) system. Simulation results suggest that: (1) When the particle size is less than 0.75 mm, the strain rate presents a double-hump shape waveform; (2) the reflection coefficient rises linearly with increasing grain-to-particle size ratio, while the transmission coefficient remains constant; and (3) increasing grain-to-particle size ratio promotes the migration of particles in grains, resulting in the decrease in crack number and dynamic tensile strength. The results show the feasibility of PFC-GBM in studying the dynamics of crystalline rock, which can provide a reference for dynamic response analysis on the microscopic scale.

**Keywords** PFC-GBM · SHPB system · SCB test · Grain-to-particle size ratio

## 1 Introduction

The tensile strength of rock is far less than the compressive strength and is inevitably disturbed by earthquake, blasting and other factors in practical engineering. Therefore, the tensile properties of rock, whose failure is often caused by complex tensile state, are the core issue under dynamic loading. Numerous studies have shown that the deformation and failure of rock are mainly controlled by its microstructure [1–3], which is associated with the mode of mineral aggregation and the amount of micro-defects, such as micro-cracks, pores and structural planes.

Due to the heterogeneity of microstructure, there are great differences in composition, geometry and strength of rock [4, 5]. To solve this problem, discontinuous methods have been increasingly used to simulate the mechanical behavior of rock. The discrete element method (DEM) has realized the research on the initiation and propagation of micro-cracks

from on the microscopic scale [6, 7]. However, it is only used to simulate rock with spheres, which has a large gap in simulating heterogeneity. In recent years, a GBM is proposed based on PFC, and the macroscopic mechanical properties of heterogeneous rock are well simulated by quantitative modeling and parameter assignment of grains. By using the PFC-GBM, the micromechanical properties of rocks and the initiation and propagation of cracks have been extensively investigated [8–10], and various influencing factors such as pre-existing cracks and grain size have also been discussed [11, 12]. The above studies show that DEM is effective in studying the mechanical properties of rocks with complex microstructure, but they focused mainly on rocks under static loading, and less on the tensile properties of heterogeneous rock and the propagation and attenuation laws of waves at high strain rates.

When using DEM to study the mechanical properties of rock at high strain rates, it is essential to characterize the microscopic grain structure and reflect its influence on the mechanical properties [13, 14]. Related studies show that grain-to-particle size ratio can significantly affect the static compressive strength and the deterioration law of mechanical properties of damaged rock [15, 16]. It is indicated that the appropriate grain and particle sizes should be selected for studies using the GBM, but the effect in dynamic tensile simulations remains to be further verified.

✉ Zhang Cong  
zcnj027@hhu.edu.cn

<sup>1</sup> Research Institute of Geotechnical Engineering, Hohai University, Nanjing 210098, Jiangsu, China

<sup>2</sup> Key Laboratory of Ministry of Education for Geomechanics and Embankment Engineering, Hohai University, Nanjing 210098, Jiangsu, China

The purpose of this research is to simulate dynamic SCB tests by using the SHPB system, where the rock is constructed based on the PFC-GBM, and then to study the influence of grain and particle sizes on the mechanical behaviors under dynamic loading such as strain rate, tensile strength and micro-cracks.

## 2 Generation of rock specimen

Voronoi diagram consists of a number of perpendicular bisectors of neighboring generators which are randomly generated [17]. It is characterized as a set of convex polygons with the following properties: (1) The distance from any point on the polygon boundary to the generator inside is equal; (2) The distance from the interior point of each polygon to the generator inside is shorter than that to other generators. The equipartition on spatial subdivision is the specific superiority of Voronoi diagram, which can be effectively used to simulate the grain structure of rock minerals.

The construction process of grain model in PFC numerical simulation is based on Voronoi diagram, which is divided into four stages (Fig. 1):

- (A) Generation of the initial generator model. As shown in Fig. 1A, each generator represents a mineral grain.
- (B) Grouping of mineral grains. As shown in Fig. 1B, construct external geometry cells according to the shape of each generator, followed by interpolation to generate the multigrain model by using Voronoi method.
- (C) Filling of grain particles. As shown in Fig. 1C, delete generators and fill each geometry with sphere particles.
- (D) Generation of structural planes. As shown in Fig. 1D, geometry cells are scaled down around their centers in equal proportions, between which particles are removed and replaced by those of different sizes and parameters.

This grain-based modeling method can not only quickly group and assign values to particles, but also conveniently adjust the size and shape of grains and structural planes. Furthermore, it ensures that the volume ratio of structural planes does not vary under different grain and particle sizes and can better simulate the interaction between grains and the initiation and propagation of microcracks.

## 3 Dynamic SCB numerical model

### 3.1 SHPB coupling system

Figure 2 shows the SHPB numerical model established by the continuous – discontinuous coupling method. To reduce the waveform oscillation, a pulse shaper (Fig. 2A) was added

to ensure that the waveform is approximately sinusoidal. The pulse shaper absorbed part of energy after being hit by the impact bar, which slowed down the decline of the loading waveform and made it smoother. Both the impact bar and pulse shaper were established using the rigid block (rblock) in PFC3D.

Compared to the Brazilian disk (BD) test, the SCB test is more prone to tensile failure with fixed initiation cracking point and crack propagation path. Thus, it is commonly used to study the fracture toughness of brittle materials such as rock [18]. To weaken the dispersion of stress wave, cushions were assigned between the specimen and bars. The specimen and cushions were built by discrete elements (ball and rblock), while the incident and transmission bars were built by continuum media, between which force and velocity were transmitted through the coupling wall (Fig. 2B and C). To avoid the great influence of the size and properties of bars on the accuracy of simulation results, the incident and transmission bars were set to 10 times the length of the impact bar to ensure that the incident and reflected waves could be captured intact.

### 3.2 Stress analysis of SCB test

Due to the complex stress conditions in the static semi-circular bending test, for which there is no analytical solution, certain simplifications are required in the stress analysis. Figure 3 shows the force diagram of the static SCB test. Assuming that the stress distribution at the mid-span section conforms to the plane section assumption, the bending moment ( $M_y$ ) and tensile stress ( $\sigma_{Oz}$ ) at point O are the maximum [19],

$$M_y = \frac{1}{4}Fl \quad (1)$$

$$\sigma_{Oz} = \frac{1.5Fl}{r^2h} \quad (2)$$

where  $F$  is the loading force at the top of the specimen,  $l$  is the spacing of the bearings on the straight side of the specimen, and  $r$  and  $h$  are, respectively, the radius and thickness of the specimen.

In the numerical simulation of dynamic SCB test, the specimen also suffers the maximum tensile stress at point O, but it has a notable gap with the theoretical value calculated according to Eq. (2). The load of the specimen in the dynamic SCB test is obtained from the incident wave ( $\sigma_i(t)$ ), reflected wave ( $\sigma_r(t)$ ) and transmitted wave ( $\sigma_t(t)$ ), where the incident and reflected waves determine the load on the left end of the specimen ( $F_1(t)$ ), and the transmitted wave determines the load on the right end of the specimen ( $F_2(t)$ ),

$$F_1(t) = [\sigma_i(t) + \sigma_r(t)]A, F_2(t) = \sigma_t(t)A \quad (3)$$

**Fig. 1** Procedures for generating generator model (A), grain structure (B), grain particles (C) and structural planes (D) of PFC-GBM

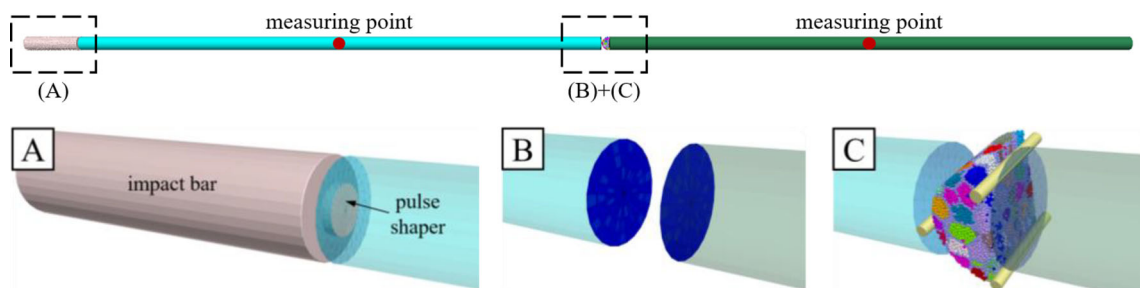
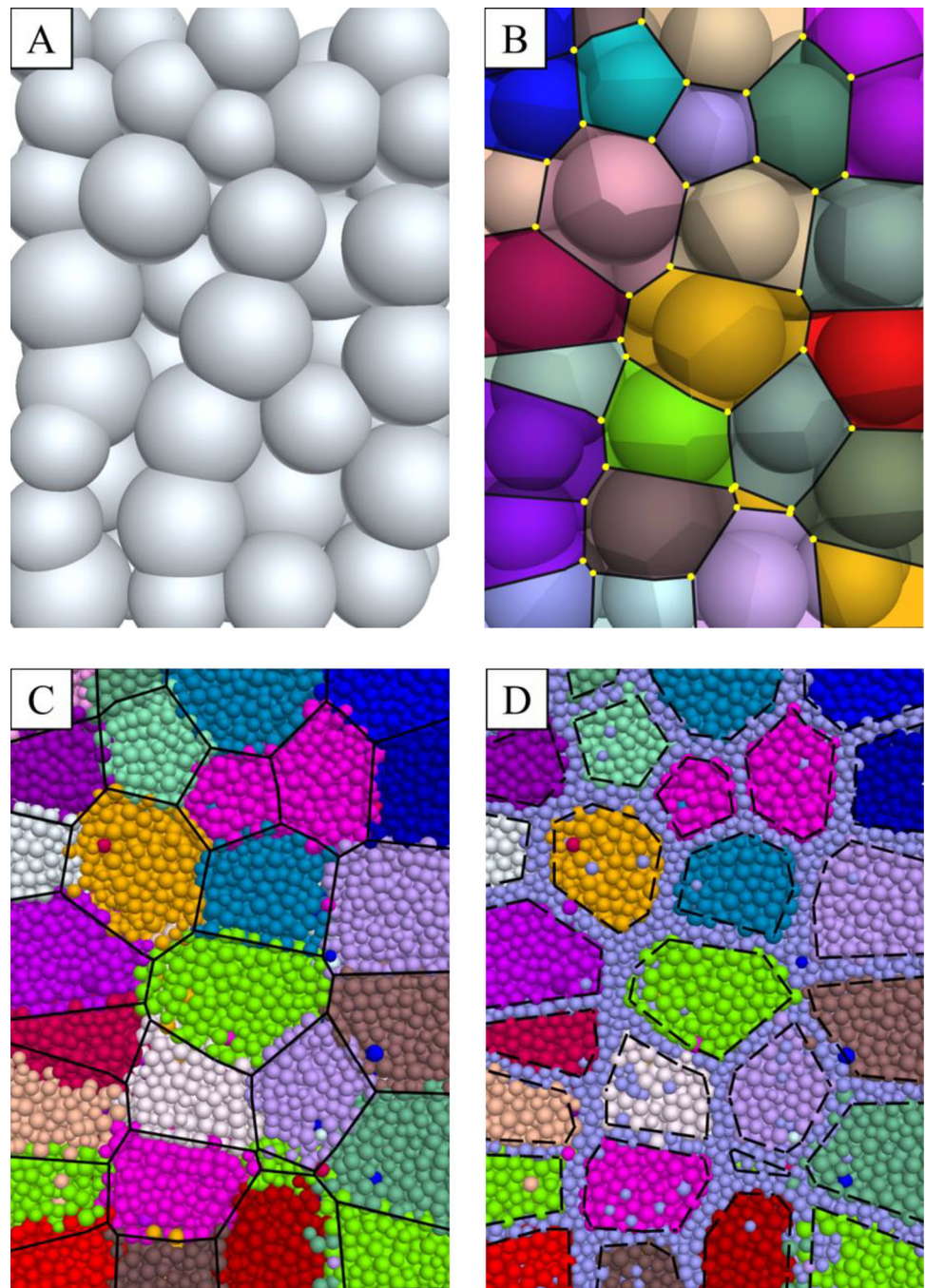


**Fig. 2** SHPB coupling system consists of launch equipment (A), wall unit (B) and rock specimen (C)

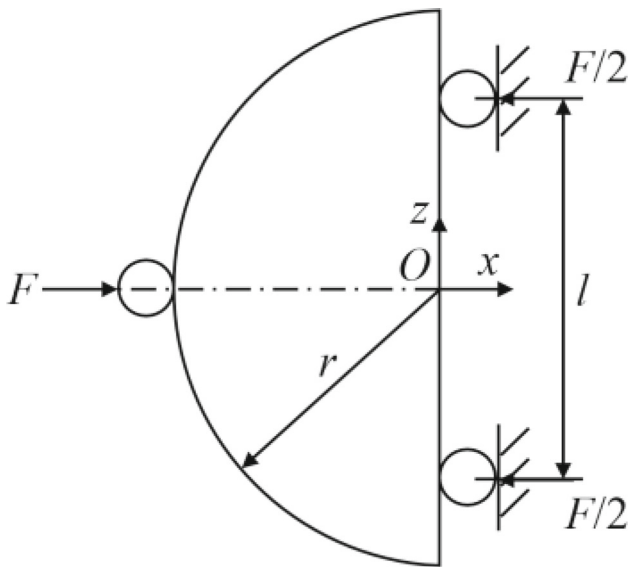


Fig. 3 Force diagram of static SCB test

where  $A$  is the cross-sectional area of bars.

Substituting Eq. (2) into Eq. (3) gives the tensile stress ( $\sigma_x(t)$ ) at point  $O$ :

$$\sigma_{x1}(t) = \frac{1.5F_1(t)l}{r^2h}, \sigma_{x2}(t) = \frac{1.5F_2(t)l}{r^2h} \quad (4)$$

The related research [20] shows that the shape and peak value of the tensile stress at point  $O$  calculated by transmitted wave ( $\sigma_{x2}(t)$ ) are closer to those of the specimen, and thus,  $\sigma_{x2}(t)$  is selected to calculate the tensile stress of the specimen.

### 3.3 Calibration of microscopic parameters

Considering the complex composition of minerals which cannot be easily grouped, a uniform value was assigned to particles for simplification. The specimen was calibrated according to the project team’s indoor test data on granite with an elastic modulus of 46.3 GPa, Poisson’s ratio of 0.33, uniaxial compressive strength of 153.5 MPa, uniaxial tensile strength of 12.0 MPa, cohesion of 20.0 MPa and internal friction angle of 60.8°. The values of microscopic parameters are shown in Table 1, where PFC soft-bond model is used for sphere particles, and FLAC elastic model is used for bar elements.

Figure 4 shows the indoor test curves and simulation curves of tensile stress-time and crack number-time of the mid-span section at impact velocity  $v = 10$  m/s. It can be seen that there is a good agreement between the two. In addition, cracks developed along and eventually penetrated the mid-span section of the specimen under tensile stress.

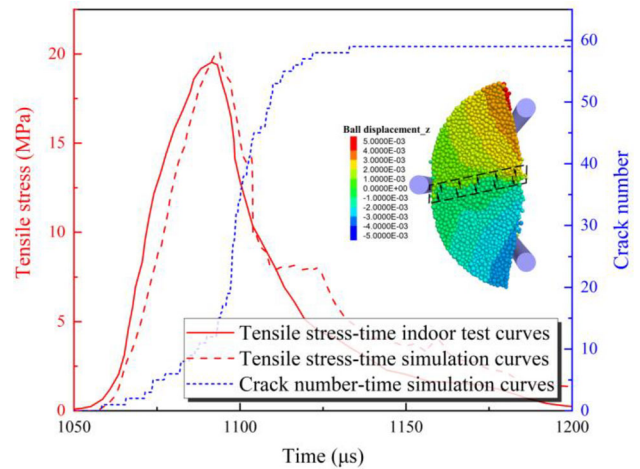


Fig. 4 Variations of tensile stress and crack number in test and simulation with time

## 4 Influence of grain-to-particle size ratio

In PFC numerical simulation, change in particle size leads to that in particle strength and surface properties, while difference in grain size leads to that in overall deformation and strength characteristics. To investigate the influence of grain size and particle size on the deformation and strength of rock specimen, numerical models with different grain sizes and particle sizes were generated for comparative tests under stress wave propagation. As shown in Fig. 5, fifteen groups of specimens were generated from A to O. The minimum particle size ( $r_{\min}$ ) is divided into three groups of 0.5 mm, 0.75 mm and 1.0 mm, and the grain-to-particle size ratio ( $R$ ) is divided into five groups of 4.0, 8.0, 12.0, 16.0 and 20.0. Figure 6 shows the tensile stress-time curves at the mid-span section of rock specimens at  $v = 10.0$  m/s, where the rotation of the pulse shaper after impact leads to different stress wave propagation velocities of the specimens.

### 4.1 Strain rate effect

It can be seen from Fig. 6 that there is a large gap between the times when specimens reached their peak tensile stresses, which is mainly due to the disturbance of the pulse shaper when it was impacted. Therefore, for the convenience of comparative analysis, the strain rate-time curves of the three specimens such as J, K and L with  $R = 16.0$  were shifted to ensure that peak strain rates were reached at the same time (Fig. 7). As shown in Fig. 7, the strain rate presents a double-hump shape waveform when  $r_{\min} = 0.5$  mm and 0.75 mm. From further analysis at the microscopic scale, as the stress wave passed through the specimen, the displacement of particles on the wave vibration surface exceeded the elastic limit of the rock, which is macroscopically manifested as plastic deformation and crack propagation. Furthermore,

**Table 1** Model microscopic mechanical parameters

PFC	Particle radius ( $r/\text{mm}$ )		Particle density ( $\rho/\text{kg}\cdot\text{m}^{-3}$ )	Effective modulus ( $E^*/\text{Gpa}$ )		Normal-to-shear stiffness ratio ( $k^*$ )
	Grains	Structural planes		Grains	Structural planes	
	1.0–1.6	0.8–1.3	3900	240.0	168.0	6.0
	Tensile strength ( $\sigma_c/\text{Mpa}$ )		Cohesion ( $c/\text{Mpa}$ )		Friction angle ( $\phi/^\circ$ )	Friction coefficient ( $\mu$ )
	Grains	Structural planes	Grains	Structural planes		
	221.0	154.7	340.0	238.0	80	1.5
	Moment-contribution factor ( $\beta$ )		Softening factor ( $\xi$ )		Softening tensile strength factor ( $\gamma$ )	
	0.6		4.0		0.7	
FLAC	Density ( $\rho/\text{kg}\cdot\text{m}^{-3}$ )		Young’s modulus ( $E/\text{Gpa}$ )		Poisson’s ratio ( $\nu$ )	
	7800		211		0.25	

the initiation of cracks reduced the contact area of the specimen, which in turn blocked the passage of the wave and thus enhanced its reflection. As a result, the second peak in strain rate-time curves occurred under the superposition of reflected and incident waves.

Figure 8 shows the variation of the peak strain rate with  $R$  for fifteen groups of specimens at  $v = 10.0$  m/s. It can be observed that the peak strain rate decreases with the increase of  $R$ , where  $R$  grows from 4.0 to 20.0, the fitted peak strain rate falls from 411.8 MPa to 384.5 MPa, with a decrease of 6.6%.

### 4.2 Reflection and transmission coefficients

In dynamic damage analysis of jointed rock under dynamic loading, reflection coefficient and transmission coefficient are important indexes to describe and measure amplitude decrement, which are used to analyze attenuation effect of stress wave through rock joint interface [21]. Reflection and transmission coefficients are generally defined as the ratios of peak strengths of reflection wave and transmission wave to that of incident wave,

$$R_p = \frac{\max|V_{RP}|}{\max|V_{IP}|}, T_p = \frac{\max|V_{TP}|}{\max|V_{IP}|} \tag{5}$$

where  $R_p$  and  $T_p$  are, respectively, the reflection and transmission coefficients,  $\max|V_{RP}|$ ,  $\max|V_{IP}|$  and  $\max|V_{TP}|$  are, respectively, the peak strengths of reflected wave, incident wave and transmitted wave.

Figure 9 shows the variations of reflection and transmission coefficients with  $R$ . As can be seen from the figure, the increase in  $R$  from 4 to 20 results in little change in the transmission coefficient from 7.7 to 7.6%, while the reflection coefficient rises linearly from 84.4 to 90.2%, with an increase of 6.9%.

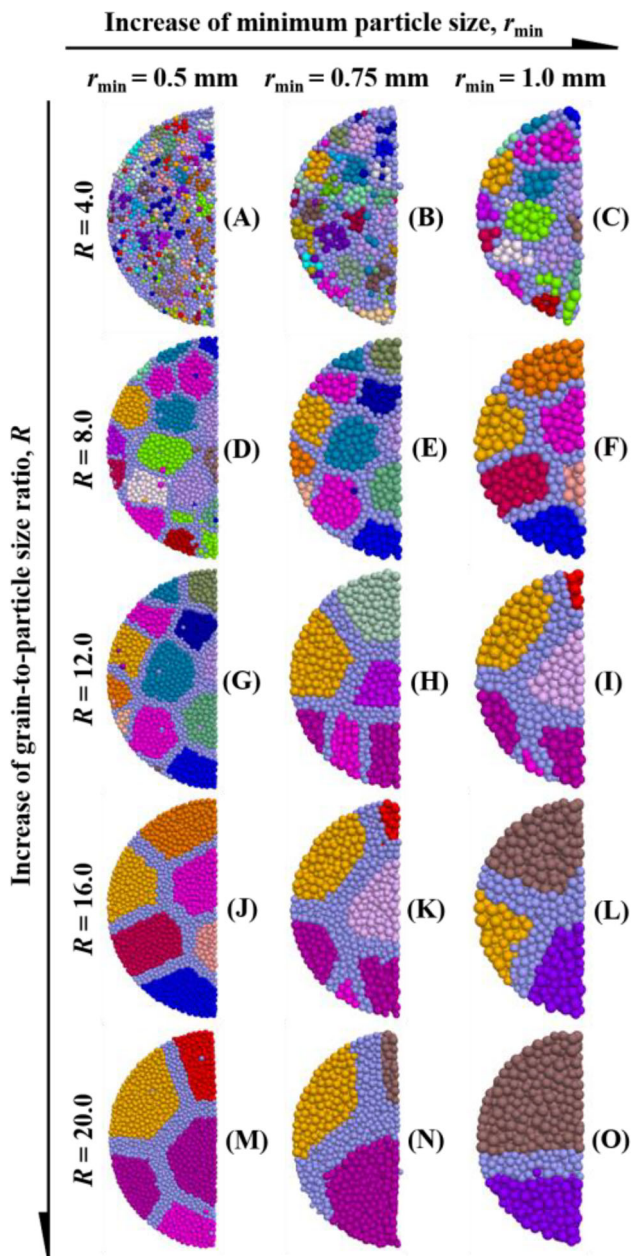
### 4.3 Dynamic tensile strength

Figure 10 reveals the variation rule of dynamic tensile strength (peak value of  $\sigma_{Oz}$ ) of specimens A–O with  $R$  at impact velocity  $v = 10$  m/s. It can be observed that the dynamic tensile strength decreases slowly with the increase of  $R$  for different particle sizes. Moreover, fitting results indicate that the decrease rate of dynamic tensile strength does not vary with particle size, where the reduction of dynamic tensile strength caused by the increase of  $R$  from 4 to 20 is approximately 16%.

## 5 Discussion

Previous studies on the rock dynamic tensile mechanical behavior were often limited to the macroscopic scale, in which the dynamic tensile strength was statistically analyzed and quantitatively described. However, there is a lack of research on the mechanical response of rock at the microscopic scale.

To further investigate the relationship between dynamic tensile properties and microstructure, the crack field of specimens during dynamic loading was analyzed. Figure 11 illustrates the bar graph of crack numbers of specimens A–O after failure, and it can be seen that the number of cracks decreases with the increase of  $R$ . Then, cracks were divided into intragranular and intergranular cracks for analysis (Fig. 12), and the ratio of intragranular cracks to total cracks gradually rises with the increase of  $R$ . Taking  $r_{\min} = 0.5$  mm as an example, when  $R$  increases from 4 to 20, the proportion of intragranular cracks soars from 22 to 53%, which is consistent with the results obtained from laboratory tests and numerical simulations by Zhang et al.[22], thus proving the rationality of using PFC-GBM method to simulate the dynamic impact effect of rock.



**Fig. 5** Numerical specimen models with different grain sizes and particle sizes

By comparing crack proportions with different particle sizes in Fig. 12A–C, it can be observed that the discreteness of data is significantly enhanced with the increase of  $r_{\min}$ , mainly due to the following reasons: (1) The increase in particle size led to the decrease in total contact number and crack number after failure, which made the simulation results more accidental; and (2) with the increase in grain-to-particle size ratio, the total number of grains comprising the specimen decreased (Fig. 5), resulting in an enhanced influence of the local microstructure on the crack proportion.

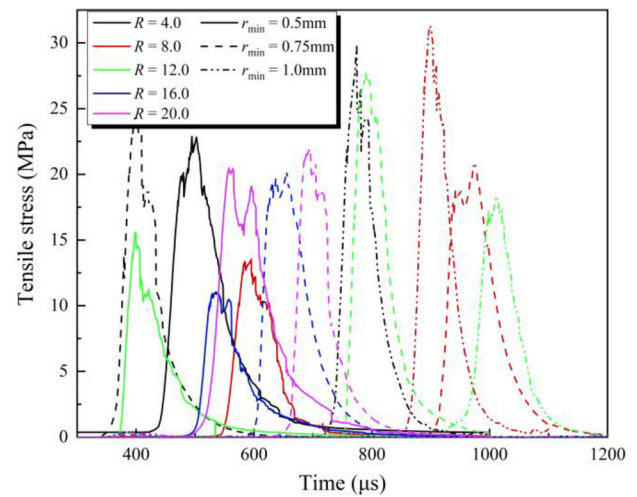


**Fig. 6** Tensile stress-time curves of the specimen with different grain sizes and particle sizes

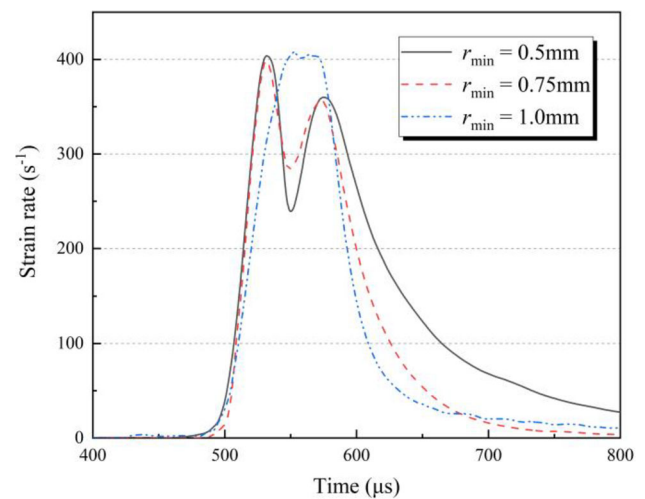


**Fig. 7** Strain rate-time curves for numerical models with different particle sizes ( $R = 16.0$ )

Considering that the crack proportion is directly related to the contact proportion, the variation of the total contact number and intragranular and intergranular contact proportions of specimens B, E, H, K, N ( $r_{\min} = 1.0$  mm) were analyzed (Fig. 13). It can be found that the total number of specimen contacts is basically constant. On the other hand, when  $R$  increases from 4 to 8, the proportion of intragranular contact grows rapidly from 25 to 37% and then goes to be flat with the increase of  $R$ , which finally stabilizes at approximately 42%.

In general, there is a direct relationship between dynamic tensile properties and grain-to-particle size ratio of specimens. The total number of cracks after failure decreases progressively with the increase of  $R$ , which reduces the energy required for deformation and failure and results in

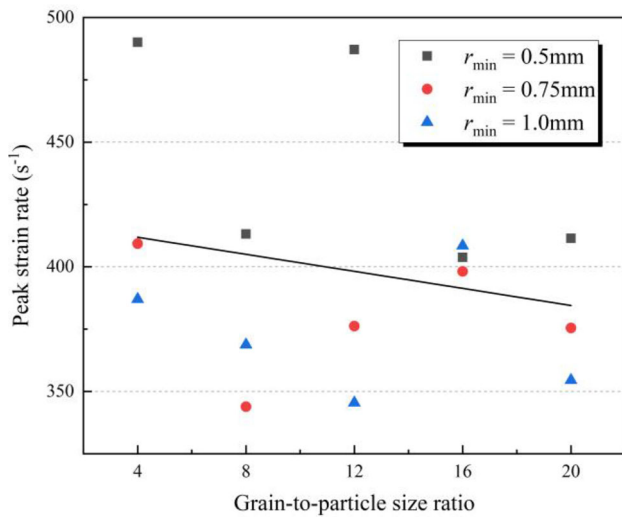


**Fig. 8** Variations of peak strain rate with grain-to-particle size ratio for numerical models with different particle sizes

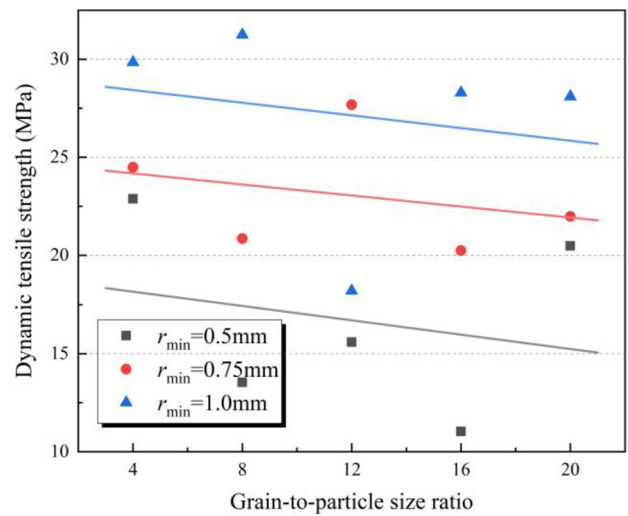


**Fig. 10** Variations of dynamic tensile strength with grain-to-particle size ratio for numerical models with different particle sizes

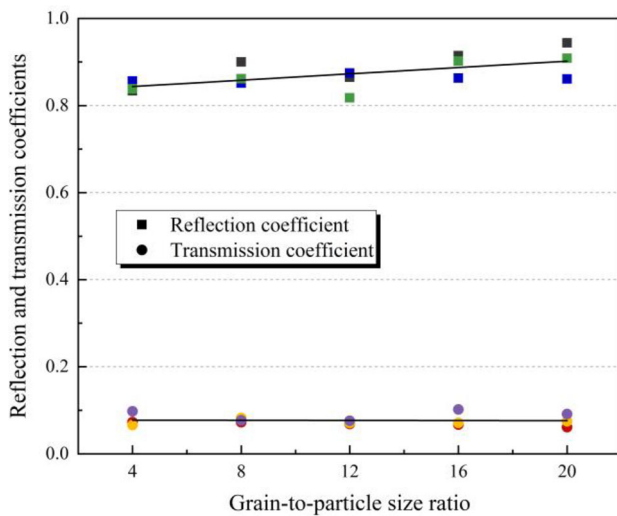


**Fig. 9** Variations of reflection and transmission coefficients with grain-to-particle size ratio for numerical models

the reduction of peak strain rate and dynamic tensile strength. While the reflection and transmission coefficients are related to the proportion of intragranular cracks after failure. With the increase of  $R$ , the proportion of intragranular cracks increases and the migration of particles in grains blocks the passage of waves, causing the reflection coefficient to rise slowly and the transmission coefficient to remain constant.

## 6 Conclusions

In this paper, the PFC-GBM and SHPB system were constructed to simulate the SCB test on rock specimens in order to study the dynamic tensile behaviors on microscopic scale.

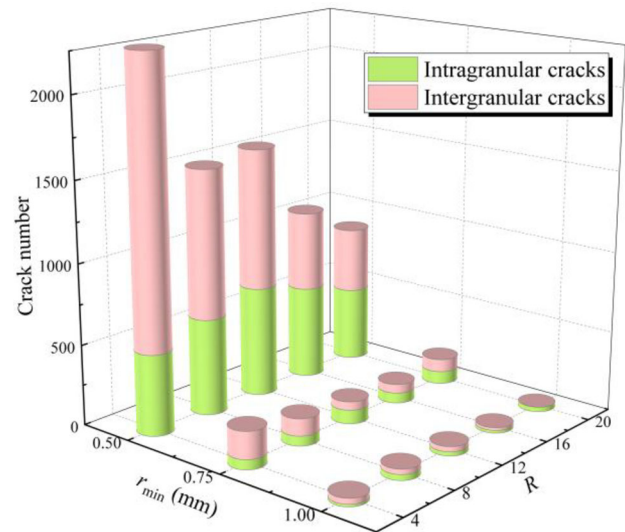


**Fig. 11** Crack number in specimens with different particle sizes and grain-to-particle size ratios

The results indicate that the microstructure of rock specimens has a massive influence on their dynamic tensile properties in numerical simulations. The primary conclusions are summarized as follows:

- (1) When the particle size is less than 0.75 mm, the coalescence and propagation of cracks block the passage and thus enhance the reflection of waves. The superposition of reflected and incident waves results in a double-hump effect on strain–time rate curves.

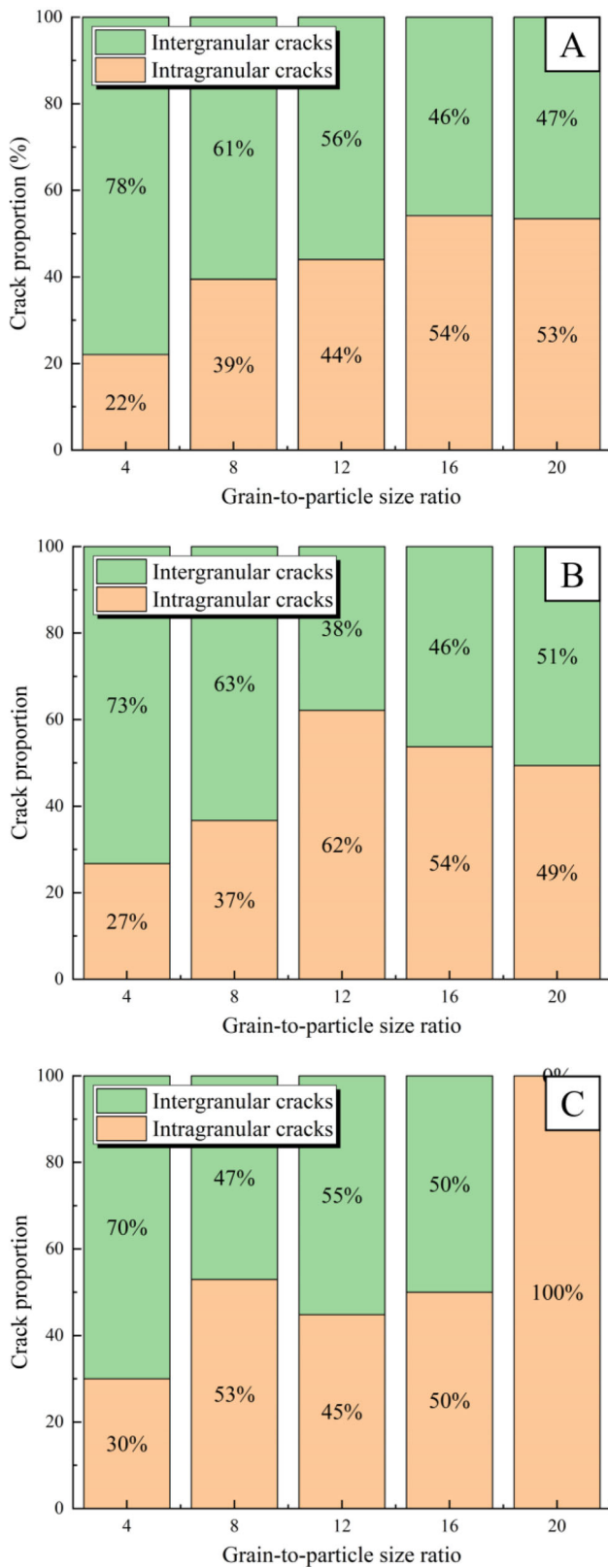


**Fig. 12** Variations of proportion of intragranular and intergranular cracks with grain-to-particle size ratio for specimens with  $r_{\min} = 0.5$  mm (A),  $r_{\min} = 0.75$  mm (B) and  $r_{\min} = 1.0$  mm (C)

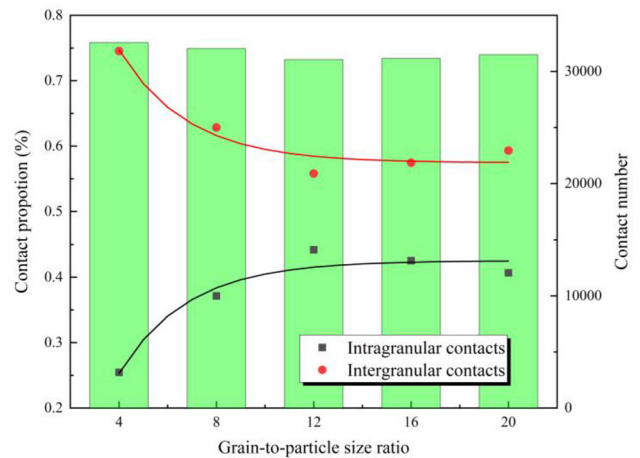


**Fig. 13** Variations of contact number and proportion of intragranular and intergranular contacts with grain-to-particle size ratio

- (2) With the increase in grain-to-particle size ratio, the dynamic tensile strength and peak strain rate of specimens decline, while the reflection coefficient rises and the transmission coefficient remains constant.
- (3) The total number of cracks after failure decreases with the increase in grain-to-particle size ratio, in which the proportion of intragranular cracks increases gradually. The intragranular structure becomes the key factor for the dynamic tensile strength of specimens.

**Acknowledgements** The work presented in this paper was financially supported by the National Key R&D Program of China (2018YFC1508501), the National Natural Science Foundation of China (Grants No. 52209130), the National Natural Science Foundation of China (Grants Nos. 41831278 and 51679071).

**Data availability** The datasets generated and/or analyzed during the current study are available from the corresponding author on reasonable request.

**Declarations**

**Conflict of interest** On behalf of all authors, the corresponding author states that there is no conflict of interest.

**References**

1. Eberhardt E, Stead D, Stimpson B, Read RS (1998) Identifying crack initiation and propagation thresholds in brittle rock. *Can Geotech J* 35(2):222–233
2. Cai M, Kaiser PK, Tasaka Y et al (2004) Generalized crack initiation and crack damage stress thresholds of brittle rock masses near underground excavations. *Int J Rock Mech Min Sci* 41(5):833–847
3. Dou LT, Yang K, Chi XL (2021) Fracture behavior and acoustic emission characteristics of sandstone samples with inclined pre-cracks. *Int J Coal Sci Technol* 8(1):77–87



4. Liu G, Chen Y, Xi D, Wang S, Fernández-Steeger TM (2022) Evolutionary analysis of heterogeneous granite microcracks based on digital image processing in grain-block model. *Materials* 15(5):1941. <https://doi.org/10.3390/ma15051941>
5. Lan HX, Martin CD, Hu B (2010) Effect of heterogeneity of brittle rock on micromechanical extensile behavior during compression loading. *J Geophys Res Solid Earth* 115(B1):B01202
6. Cundall PA, Strack ODL (2008) A discrete numerical model for granular assemblies. *Géotechnique* 30(3):331–336
7. Wang G, Luo Y, Li XP et al (2022) Study on dynamic mechanical properties and meso-damage mechanism of jointed rock under impact load. *Eur J Environ Civ Eng* 26(3):1141–1157
8. Hofmann H, Babadagli T, Zimmermann G (2015) A grain based modeling study of fracture branching during compression tests in granites. *Int J Rock Mech Min Sci* 77:152–162
9. Peng J, Wong LNY, Teh CI et al (2018) Modeling micro-cracking behavior of bukit timah granite using grain-based model. *Rock Mech Rock Eng* 51(1):135–154
10. Li H, Ma HL, Shi XL et al (2020) A 3D grain-based model for simulating the micromechanical behavior of salt rock. *Rock Mech Rock Eng* 53(3):2819–2837
11. Saadat M, Taheri A (2019) A numerical approach to investigate the effects of rock texture on the damage and crack propagation of a pre-cracked granite. *Comput Geotech* 111:89–111
12. Zhang XP, Ji PQ, Peng J et al (2020) A grain-based model considering pre-existing cracks for modelling mechanical properties of crystalline rock. *Comput Geotech* 127(5):103776
13. Liu XQ, Wang G, Liu TT et al (2020) Study on dynamic mechanical properties of phosphate rock through experimental tests and mesoscale simulation. *Arab J Geosci* 13(18):969
14. Gong FQ, Si XF, Li XB et al (2019) Dynamic triaxial compression tests on sandstone at high strain rates and low confining pressures with split Hopkinson pressure bar. *Int J Rock Mech Min Sci* 113:211–219
15. Peng J, Wong LNY, Teh CI (2017) Effects of grain size-to-particle size ratio on micro-cracking behavior using a bonded-particle grain-based model. *Int J Rock Mech Min Sci* 100:207–217
16. Tian WL, Yang SQ, Huang YH et al (2020) Mechanical behavior of granite with different grain sizes after high-temperature treatment by particle flow simulation. *Rock Mech Rock Eng* 53(3):1–17
17. Lv YX, Li HB, Zhu XH et al (2017) Discrete element method simulation of random Voronoi grain-based models. *Clust Comput* 20(1):335–345
18. Chong KP, Kuruppu MD (1984) New specimen for fracture toughness determination for rock and other materials. *Int J Fract* 26(2):R59–R62
19. Molenaar J, Molenaar A (2000) Fracture toughness of asphalt in the semi-circular bend test. In: Proceedings of the papers submitted for review at 2nd Eurasphalt and Eurobitume congress, September 20–22, Barcelona, Spain, Book 1-Session 1
20. Geng NN (2013) Numerical simulation of Semi-circular bending test for concrete under quasi-static and dynamic loading conditions. Hefei University of Technology (**In Chinese**)
21. Chen X, Li JC, Cai MF et al (2015) Experimental study on wave propagation across a rock joint with rough surface. *Rock Mech Rock Eng* 48(6):2225–2234
22. Zhang T, Wei LY, Ju MH et al (2022) Study on the effect of grain size-particle size ratio on the dynamic tensile properties of granite based on PFC3D-GBM. *Chin J Rock Mech Eng* 41(3):468–478 (**In Chinese**)

**Publisher's Note** Springer Nature remains neutral with regard to jurisdictional claims in published maps and institutional affiliations.

Springer Nature or its licensor (e.g. a society or other partner) holds exclusive rights to this article under a publishing agreement with the author(s) or other rightsholder(s); author self-archiving of the accepted manuscript version of this article is solely governed by the terms of such publishing agreement and applicable law.